

## THE H $\alpha$ LUMINOSITY FUNCTION AND STAR FORMATION RATE AT $z \approx 0.24$ IN THE COSMOS 2 SQUARE DEGREE FIELD<sup>1</sup>

Y. SHIOYA,<sup>2</sup> Y. TANIGUCHI,<sup>2</sup> S. S. SASAKI,<sup>3,4,5</sup> T. NAGAO,<sup>6</sup> T. MURAYAMA,<sup>4</sup> M. I. TAKAHASHI,<sup>4</sup> M. AJIKI,<sup>4</sup> Y. IDEUE,<sup>3</sup> S. MIHARA,<sup>3</sup>  
 A. NAKAJIMA,<sup>3</sup> N. Z. SCOVILLE,<sup>5,7</sup> B. MOBASHER,<sup>8</sup> H. AUSSSEL,<sup>7,9</sup> M. GIAVALISCO,<sup>8</sup> L. GUZZO,<sup>10</sup> G. HASINGER,<sup>11</sup> C. IMPEY,<sup>12</sup>  
 O. LE FÈVRE,<sup>13</sup> S. LILLY,<sup>14</sup> A. RENZINI,<sup>15</sup> M. RICH,<sup>16</sup> D. B. SANDERS,<sup>7</sup> E. SCHINNERER,<sup>17</sup> P. SHOPBELL,<sup>5</sup>  
 A. LEAUTHAUD,<sup>13</sup> J.-P. KNEIB,<sup>5,13</sup> J. RHODES,<sup>5</sup> AND R. MASSEY<sup>5,18</sup>

Received 2006 September 10; accepted 2007 September 5

### ABSTRACT

To derive a new H $\alpha$  luminosity function and to understand the clustering properties of star-forming galaxies at  $z \approx 0.24$ , we have made a narrowband imaging survey for H $\alpha$ -emitting galaxies in the *Hubble Space Telescope* (HST) COSMOS 2 square degree field. We used the narrowband filter NB816 ( $\lambda_c = 8150$  Å,  $\Delta\lambda = 120$  Å) and sampled H $\alpha$  emitters with  $\text{EW}_{\text{obs}}(\text{H}\alpha + [\text{N II}]) > 12$  Å in a redshift range between  $z = 0.233$  and  $0.251$  corresponding to a depth of 70 Mpc. We obtained 980 H $\alpha$ -emitting galaxies in a sky area of 5540 arcmin<sup>2</sup>, corresponding to a survey volume of  $3.1 \times 10^4$  Mpc<sup>3</sup>. We derive a H $\alpha$  luminosity function with a best-fit Schechter function parameter set of  $\alpha = -1.35^{+0.11}_{-0.13}$ ,  $\log \phi_* = -2.65^{+0.27}_{-0.38}$ , and  $\log L_*(\text{ergs s}^{-1}) = 41.94^{+0.38}_{-0.23}$ . The H $\alpha$  luminosity density is  $2.7^{+0.7}_{-0.6} \times 10^{39}$  ergs s<sup>-1</sup> Mpc<sup>-3</sup>. After subtracting the AGN contribution (15%) to the H $\alpha$  luminosity density, the star formation rate density is evaluated as  $1.8^{+0.7}_{-0.4} \times 10^{-2} M_\odot \text{ yr}^{-1} \text{ Mpc}^{-3}$ . The angular two-point correlation function of H $\alpha$ -emitting galaxies of  $\log L(\text{H}\alpha) > 39.8$  is well fit by a power-law form of  $w(\theta) = 0.013^{+0.002}_{-0.001} \theta^{-0.88 \pm 0.03}$ , corresponding to the correlation function of  $\xi(r) = (r/1.9 \text{ Mpc})^{-1.88}$ . We also find that the H $\alpha$  emitters with higher H $\alpha$  luminosity are more strongly clustered than those with lower luminosity.

**Subject headings:** galaxies: distances and redshifts — galaxies: evolution —  
 galaxies: luminosity function, mass function

**Online material:** machine-readable table

### 1. INTRODUCTION

It is important to understand when and where intense star formation occurred during the course of galaxy evolution. Although the star formation history in individual galaxies is interesting, a general trend of star formation in galaxies as a function of time

(or redshift) also provides important insights on the global star formation history as well as on the metal enrichment history in the universe. Therefore, the star formation rate density (SFRD) is one of the important observables for our understanding of galaxy formation and evolution. In the last decade, many works have followed the pioneer work of Madau et al. (1996), which compiled the evolution of SFRD,  $\rho_{\text{SFR}}$ , as a function of redshift for the first time. The evolution of  $\rho_{\text{SFR}}$  is now widely accepted as follows:  $\rho_{\text{SFR}}$  steeply increases from  $z \simeq 0$  to  $z \sim 1$ , and seems to be constant between  $z \sim 2$  and  $z \sim 5$  and may decline beyond  $z \sim 5$  (Hopkins 2004 and references therein; Giavalisco et al. 2004; Taniguchi et al. 2005; Bouwens & Illingworth 2006).

Recent observations by the *Galaxy Evolution Explorer* (GALEX) and the *Spitzer Space Telescope* have confirmed that  $\rho_{\text{SFR}}$  increases from  $z \sim 0$  to  $z \sim 1$  (e.g., Schiminovich et al. 2005; Le Floch et al. 2005). However, their observations show that the IR luminosity density evolves as  $(1+z)^4$ , while the UV luminosity density evolves as  $(1+z)^{2.5}$ . This may imply that extinction by dust and reradiation from dust becomes to play a more important role at higher redshift. One of the remaining problems in this field is a relation between star formation activity and large-scale structure formation. To study this issue, wide-field deep surveys are important.

There are several star formation rate (SFR) estimators, e.g., UV continuum, H $\alpha$  emission, [O II] emission, far-infrared (FIR) emission (Kennicutt 1998), and radio continuum (Condon 1992). Each estimator has both advantages and disadvantages to estimate the SFR. UV continuum and nebular emission lines are considered to be direct tracers of hot massive young stars. However, they are often affected by dust obscuration. On the other hand, FIR and radio continuum are insensitive to dust obscuration. FIR emission is due to the dust heated by the general interstellar radiation field. If most of the bolometric luminosity of a galaxy absorbed by dust

<sup>1</sup> Based on data collected at Subaru Telescope, which is operated by the National Astronomical Observatory of Japan.

<sup>2</sup> Research Center for Space and Cosmic Evolution, Ehime University, Bunkyo-cho, Matsuyama 790-8577, Japan.

<sup>3</sup> Graduate School of Science and Engineering, Ehime University, Bunkyo-cho, Matsuyama 790-8577, Japan.

<sup>4</sup> Astronomical Institute, Graduate School of Science, Tohoku University, Aramaki, Aoba, Sendai 980-8578, Japan.

<sup>5</sup> Department of Astronomy, MS 105-24, California Institute of Technology, Pasadena, CA 91125.

<sup>6</sup> National Astronomical Observatory of Japan, Mitaka, Tokyo 181-8588, Japan.

<sup>7</sup> Institute for Astronomy, University of Hawaii, 2680 Woodlawn Drive, Honolulu, HI 96822.

<sup>8</sup> Space Telescope Science Institute, 3700 San Martin Drive, Baltimore, MD 21218.

<sup>9</sup> CEA Saclay, DSM/DAPNIA/SAP, 91191 Gif-sur-Yvette Cedex, France.

<sup>10</sup> Osservatorio Astronomico di Brera, via Brera, Milan, Italy.

<sup>11</sup> Max-Planck-Institut für Extraterrestrische Physik, D-85478 Garching, Germany.

<sup>12</sup> Steward Observatory, University of Arizona, 933 North Cherry Avenue, Tucson, AZ 85721.

<sup>13</sup> Laboratoire d'Astrophysique de Marseille, BP 8, Traverse du Siphon, 13376 Marseille Cedex 12, France.

<sup>14</sup> Department of Physics, Swiss Federal Institute of Technology (ETH-Zurich), CH-8093 Zurich, Switzerland.

<sup>15</sup> European Southern Observatory, Karl-Schwarzschild-Strasse 2, D-85748 Garching, Germany.

<sup>16</sup> Department of Physics and Astronomy, University of California, Los Angeles, CA 90095.

<sup>17</sup> Max-Planck-Institut für Astronomie, Königstuhl 17, D-69117 Heidelberg, Germany.

<sup>18</sup> Jet Propulsion Laboratory, Pasadena, CA 91109.

is radiated from young stars, as in the case of dusty starbursts, the FIR luminosity is a good SFR estimator. For early-type galaxies, much of the FIR emission is considered to be related to the old stars and the FIR emission is not a good SFR estimator (Sauvage & Thuan 1992; Kennicutt 1998). For star-forming galaxies, there is a tight radio-FIR correlation (Condon 1992). This relation suggests that the radio continuum also provides a good SFR estimator. The radio continuum is considered to be dominated by synchrotron radiation from relativistic electrons, which are accelerated in supernova remnants (SNRs; Lequeux 1971; Kennicutt 1983a; Gavazzi et al. 1986). We note that the radio continuum emission of some galaxies is dominated by the AGN component, although such galaxies are distinguished from star-forming galaxies by using the tight radio-FIR correlation (Sopp & Alexander 1991; Condon 1992). The nearly linear radio-FIR correlation also suggests that the radio continuum is affected by the efficiency of cosmic-ray confinement, since the degree of dust attenuation becomes larger for more luminous galaxies (Bell 2003). Although SFRs evaluated from different SFR estimators are consistent with each other within a factor of 3 if the appropriate correction is applied for each case (e.g., Hopkins et al. 2003; Charlot & Longhetti 2001; Charlot et al. 2002), samples selected with a different method may have different biases. For example, samples selected by an objective-prism imaging survey are biased toward the systems with large equivalent width (e.g., Gallego et al. 1995), while those selected by UV radiation are biased against heavily dusty galaxies (Meurer et al. 2006). To evaluate the true SFRD, it is important to correct the obtained SFR appropriately and to know probable biases for the sample selection.

In this work, we use the H $\alpha$  luminosity as a SFR estimator. The H $\alpha$  luminosity is directly connected to the ionizing photon production rate. There are two approaches to measure H $\alpha$  luminosities of galaxies. One is a spectroscopic survey, and the other is a narrowband imaging survey. Although spectroscopic observations tell us details of emission line properties, e.g., Balmer decrement, metallicity, and so on, it is difficult to obtain spectra of a large sample of faint galaxies. On the other hand, narrowband imaging observations make it possible to measure an emission-line flux of galaxies over a wide field of view. Another advantage of narrowband imaging is that aperture corrections do not need to evaluate the total flux of H $\alpha$  emission. However, there are some shortcomings with this method: e.g., a narrowband filter cannot separate H $\alpha$  emission from [N II]  $\lambda\lambda 6548, 6583$  emission, and we cannot evaluate the obscuration degree for each galaxy. Therefore, we must correct these effects statistically. Since the redshift coverage of emission-line galaxies discovered by the narrowband imaging method is restricted, the survey volume of emission-line galaxies is small. Therefore, it is difficult to obtain a large sample of H $\alpha$  emitters. If this is the case, brighter (i.e., rarer) H $\alpha$  emitters could be missed in such an imaging survey. In order to study the H $\alpha$  luminosity function unambiguously, we need a large sample of H $\alpha$  emitters covering a wide range of H $\alpha$  luminosity. On the other hand, this restriction allows us to investigate large-scale structures of emission-line galaxies (mostly, star-forming galaxies) at a concerned redshift slice.

Motivated by this in part, we have carried out a narrowband imaging survey of the *HST* COSMOS field centered at  $\alpha(\text{J2000.0}) = 10^{\text{h}}00^{\text{m}}28.6^{\text{s}}$  and  $\delta(\text{J2000.0}) = +02^{\circ}12'21.0''$  (the Cosmic Evolution Survey; Scoville et al. 2007). Since this field covers  $2 \text{ deg}^2$ , it is suitable for our purpose. Our optical narrowband imaging observations of the *HST* COSMOS field have been made with the Suprime-Cam (Miyazaki et al. 2002) on the Subaru Telescope (Kaifu et al. 2000; Iye et al. 2004). Since the Suprime-Cam consists of  $10 \text{ k} \times 4 \text{ k}$  CCD chips and provides a very wide field

of view ( $34' \times 27'$ ), this is suitable for any wide-field optical imaging surveys. In our observations, we used the narrow-passband filter, NB816, centered at  $8150 \text{ \AA}$  with the passband of  $\Delta\lambda = 120 \text{ \AA}$ . Our NB816 imaging data are also used to search both for Ly $\alpha$  emitters at  $z \approx 5.7$  (Murayama et al. 2007) and for [O II] emitters at  $z \approx 1.2$  (Takahashi et al. 2007). In this paper, we present our results on H $\alpha$  emitters at  $z \approx 0.24$  in the *HST* COSMOS field.

Throughout this paper, magnitudes are given in the AB system. We adopt a flat universe with  $\Omega_{\text{matter}} = 0.3$ ,  $\Omega_{\Lambda} = 0.7$ , and  $H_0 = 70 \text{ km s}^{-1} \text{ Mpc}^{-1}$ .

## 2. PHOTOMETRIC CATALOG

In this analysis, we use the COSMOS official photometric redshift catalog, which includes objects whose total  $i$  magnitudes ( $i'$  or  $i^*$ ) are brighter than 25. The catalog presents  $3''$  diameter aperture magnitude of Subaru Suprime-Cam  $B, V, r', i', z'$ , and NB816.<sup>19</sup> Details of the Suprime-Cam observations are given in Taniguchi et al. (2007). Details of the COSMOS official photometric redshift catalog is also described in Capak et al. (2007) and Mobasher et al. (2007). Since the accuracy of standard star calibration ( $\pm 0.05 \text{ mag}$ ) is too large to obtain an accurate photometric redshift, Capak et al. (2007) recalibrated the photometric zero points for photometric redshift using the SEDs of galaxies with spectroscopic redshift. Following the recommendation of Capak et al. (2007), we apply the zero-point correction to the photometric data in the official catalog. The offset values are 0.189, 0.04,  $-0.040$ ,  $-0.020$ , 0.054, and  $-0.072$  for  $B, V, r', i', z'$ , and NB816, respectively. The zero-point-corrected limiting magnitudes are  $B = 27.4$ ,  $V = 26.5$ ,  $r' = 26.6$ ,  $i' = 26.1$ ,  $z' = 25.4$ , and NB816 = 25.6 for a  $3 \sigma$  detection on a  $3''$  diameter aperture. The catalog also includes  $3''$  diameter aperture magnitude of CFHT  $i^*$ . We use the CFHT  $i^*$  magnitude for bright galaxies with  $i' < 21$  because such bright galaxies appear to be slightly affected by the saturation effect in  $i'$  obtained with Suprime-Cam. We also apply the Galactic extinction correction adopting the median value  $E(B - V) = 0.0195$  (Capak et al. 2007) for all objects. A photometric correction for each band is as follows (see Table 8 of Capak et al. 2007):  $A_B = 0.079$ ,  $A_V = 0.061$ ,  $A_{r'} = 0.050$ ,  $A_{i'} = 0.037$ ,  $A_{z'} = 0.028$ ,  $A_{\text{NB816}} = 0.034$ , and  $A_{i^*} = 0.037$ .

## 3. RESULTS

### 3.1. Selection of NB816-Excess Objects

We select H $\alpha$  emitter candidates using  $3''$  diameter aperture magnitude in the official catalog. In order to select NB816-excess objects efficiently, we need the magnitude of a frequency-matched continuum. Since the effective frequency of the NB816 filter (367.8 THz) is different either from those of the  $i'$  (394.9 THz) and  $z'$  (333.6 THz) filters, we make new a frequency-matched continuum, the “ $iz$  continuum,” using the following linear combination;  $f_{iz} = 0.57f_{i'} + 0.43f_{z'}$ , where  $f_{i'}$  and  $f_{z'}$  are the  $i'$  and  $z'$  flux densities, respectively. Its  $3 \sigma$  limiting magnitude is  $iz \simeq 26.03$  in a  $3''$  diameter aperture. For the bright galaxies with  $i' < 21$ , the “ $iz$  continuum” is calculated as  $f_{iz} = 0.57f_{i^*} + 0.43f_{z'}$ , where  $f_{i^*}$  is the  $i^*$  flux density, since the  $i'$  magnitude is incorrect because of the saturation effect.

Since we use the ACS catalog prepared for studying weak lensing (Leauthaud et al. 2007) to separate galaxies from stars, our survey area is restricted to the area mapped in the  $I_{814}$  band with the Advanced Camera for Surveys (ACS) on *HST*. After subtracting

<sup>19</sup> Our SDSS broadband filters are designated as  $g^+$ ,  $r^+$ ,  $i^+$ , and  $z^+$  in Capak et al. (2007) to distinguish them from the original SDSS filters. Also, our  $B$  and  $V$  filters are designated as  $B_J$  and  $V_J$  in Capak et al. (2007), where “J” means the Johnson and Cousins filter system used in Landolt (1992).

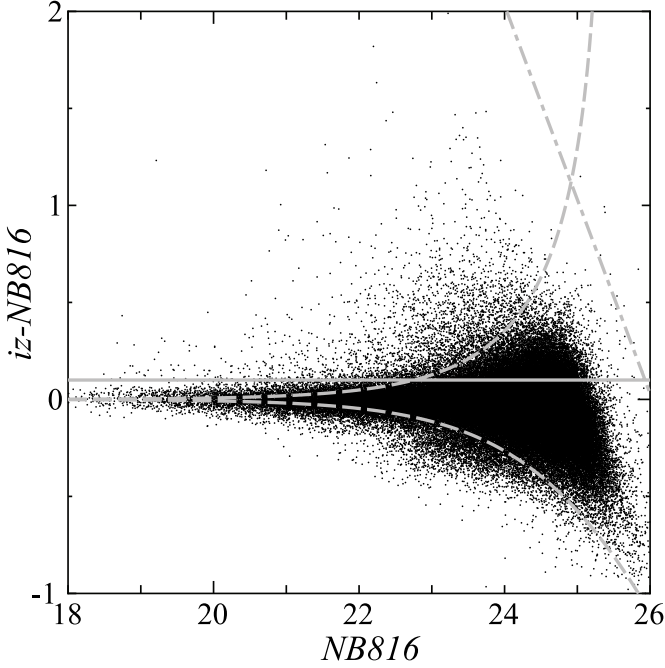


FIG. 1.—Diagram of  $iz - \text{NB816}$  vs.  $\text{NB816}$  for all objects classified as galaxies in the ACS catalog. The horizontal solid line corresponds to  $iz - \text{NB816} = 0.1$ . The dashed lines show the distribution of  $3\sigma$  error. The dot-dashed line shows the limiting magnitude of  $iz$ . Since the total  $i'$ -magnitudes of galaxies in the official photometric redshift catalog are brighter than 25,  $iz$  magnitudes of most of them are brighter than the limiting magnitude.

the masked-out area, the effective survey area is 5540 arcmin<sup>2</sup>. Since the covered redshift range is between 0.233 and 0.251 ( $\Delta z = 0.018$ ) and the corresponding survey depth is 70 Mpc, our effective survey volume is  $3.1 \times 10^4 \text{ Mpc}^3$ .

We selected NB 816-excess objects using the following criteria:

$$iz - \text{NB816} > 0.1 \quad (1)$$

and

$$iz - \text{NB816} > 3\sigma(iz - \text{NB816}), \quad (2)$$

where

$$3\sigma(iz - \text{NB816}) = -2.5 \log \left[ 1 - \sqrt{(f_{3\sigma_{\text{NB816}}})^2 + (f_{3\sigma_{iz}})^2 / f_{\text{NB816}}} \right]. \quad (3)$$

In the calculation of  $3\sigma(iz - \text{NB816})$ , we applied the Galactic extinction correction to the limiting magnitudes of the  $i'$  and  $z'$  bands. The former criterion corresponds  $\text{EW}_{\text{obs}} > 12 \text{ \AA}$ . This criterion is exactly same as that of Fujita et al. (2003) and similar to that of Tresse & Maddox (1998) [ $\text{EW}(\text{H}\alpha + [\text{N II}])_{\text{rest}} > 10 \text{ \AA}$ ]. Taking account of the scatter of the  $iz - \text{NB816}$  color, we added the latter criterion. These two criteria are shown by the solid and dashed lines, respectively, in Figure 1. As we will describe in the next section, we use the broadband colors of galaxies to separate  $\text{H}\alpha$  emitters from other emission-line galaxies. To avoid the ambiguity of broadband colors, we select galaxies detected above  $3\sigma$  in all bands. Finally, we find 6176 galaxies that satisfy the above criteria.

### 3.2. Selection of NB816-Excess Objects at $z \approx 0.24$

The emission-line galaxy candidates selected above include not only  $\text{H}\alpha$  emitters at  $z = 0.24$ , but also possibly  $[\text{O III}]$  emitters

at  $z = 0.63$ , or  $\text{H}\beta$  emitters at  $z = 0.68$ , or  $[\text{O II}]$  emitters at  $z = 1.19$  (Tresse et al. 1999; Kennicutt 1992b). We also note here that the narrowband filter passband is too wide to separate  $[\text{N II}] \lambda\lambda 6548, 6583$  from  $\text{H}\alpha$ .

In order to distinguish  $\text{H}\alpha$  emitters at  $z \approx 0.24$  from emission-line objects at other redshifts, we investigate their broadband color properties by comparing the observed colors of our 6176 emitters with model ones that are estimated by using the model spectral energy distribution derived by Coleman et al. (1980). In Figures 2 and 3, we show the  $B - V$  versus  $V - r'$  and  $B - r'$  versus  $i' - z'$  color-color diagrams of the 6176 sources and the loci of model galaxies. Then we find that  $\text{H}\alpha$  emitters at  $z \approx 0.24$  can be selected by adopting the following three criteria: (1)  $B - V > 2(V - r') - 0.2$ ; (2)  $B - r' > 5(i' - z') - 1.3$ ; and (3)  $B - r' > 0.7(i' - z') + 0.4$ . We can clearly distinguish  $\text{H}\alpha$  emitters from  $[\text{O III}]$  or  $\text{H}\beta$  emitters using the first criterion. We can also distinguish  $\text{H}\alpha$  emitters from  $[\text{O II}]$  emitters using the second and third criteria. We have checked the validity of our photometric selection criteria using both the photometric data and spectroscopic redshifts of galaxies in the GOODS-N region (Cowie et al. 2004). Galaxies with redshifts corresponding to our  $\text{H}\alpha$ ,  $[\text{O III}]$ ,  $\text{H}\beta$ , and  $[\text{O II}]$  emitters are separately plotted in Figures 2 and 3. It is shown that our criteria can well separate  $\text{H}\alpha$  emitters from  $[\text{O III}]$ ,  $\text{H}\beta$ , and  $[\text{O II}]$  emitters. These criteria give us a sample of 981  $\text{H}\alpha$ -emitting galaxy candidates. The properties of GOODS-N galaxies presented in Figures 2 and 3 suggest that there is little contamination in our  $\text{H}\alpha$  emitter sample.

### 3.3. $\text{H}\alpha$ Luminosity

As we mentioned in § 1, one of the advantages of narrowband imaging is to measure the total flux of  $\text{H}\alpha$  emission directly without any aperture correction. To derive the total  $\text{H}\alpha$  flux, we have used the total flux of  $i'$  (or  $i^*$ ),  $z'$ , and NB816 using public images.<sup>20</sup> Our procedure is the same as that given in Capak et al. (2007): MAG\_AUTO in SExtractor (Bertin & Arnouts 1996). Because of the contamination of the foreground galaxies, one galaxy has a negative value of  $iz - \text{NB816}$  based on the total magnitudes. We do not use this object in further analysis. Therefore, our final sample contains 980  $\text{H}\alpha$  emitters.

Adopting the same method as that used by Pascual et al. (2001), we express the flux density in each filter band as the sum of the line flux,  $F_L$ , and the continuum flux density,  $f_C$ :

$$f_{\text{NB}} = f_C + \frac{F_L}{\Delta \text{NB}}, \quad (4)$$

$$f_{i'} = f_C + \frac{F_L}{\Delta i'}, \quad (5)$$

$$f_{z'} = f_C, \quad (6)$$

where  $\Delta \text{NB}$  and  $\Delta i'$  are the effective bandwidths of NB816 and  $i'$ , respectively. The  $iz$  continuum,  $f_{iz}$ , is expressed as

$$f_{iz} = 0.57f_{i'} + 0.43f_{z'} = f_C + 0.57 \frac{F_L}{\Delta i'}. \quad (7)$$

Using equations (4) and (7), the line flux  $F_L$  is calculated by

$$F_L = \Delta \text{NB} \frac{f_{\text{NB}} - f_{iz}}{1 - 0.57(\Delta \text{NB} / \Delta i')}. \quad (8)$$

The line flux evaluated above includes both  $\text{H}\alpha$  and  $[\text{N II}] \lambda\lambda 6548, 6583$  emission since the narrowband filter cannot separate

<sup>20</sup> See <http://irsa.ipac.caltech.edu/data/COSMOS/>.

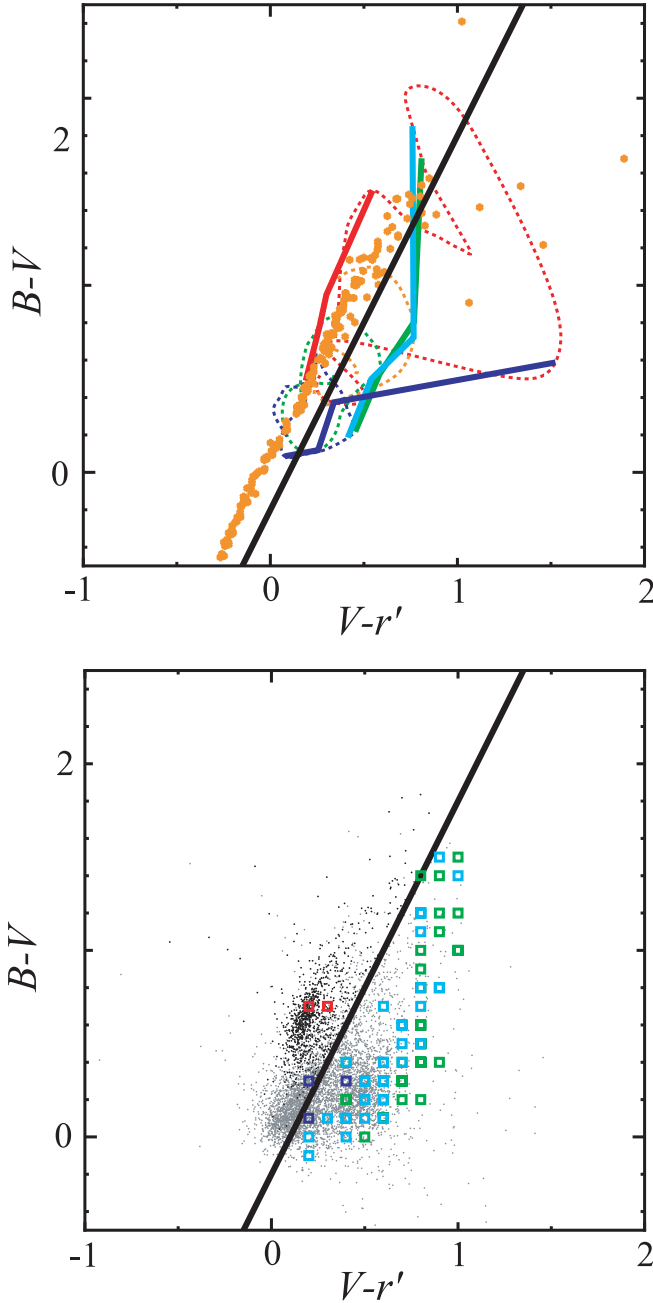


FIG. 2.—Diagrams of  $B - V$  vs.  $V - r'$ . *Top*: Colors of model galaxies (CWW) from  $z = 0$  to  $z = 3$  are shown with dotted lines: red, orange, green, and blue lines show the loci of E, Sbc, Scd, and Irr galaxies, respectively. Colors of  $z = 0.24, 0.64, 0.68$ , and  $1.18$  (for  $H\alpha$ ,  $[O III]$ ,  $H\beta$ , and  $[O II]$  emitters, respectively) are shown with red, green, light blue, and blue lines, respectively. Orange asterisks show the star of Gunn & Stryker (1983). *Bottom*: Plot of  $B - V$  vs.  $V - r'$  for the 6176 sources found with emitter selection criteria. In this diagram,  $H\alpha$  emitters are located above the black line, which is adopted by us as one of the criteria for the selection of  $H\alpha$  emitters. The 980  $H\alpha$  emitters are shown as black dots, and other emission-line galaxy candidates are shown as gray dots. Galaxies in GOODS-N (Cowie et al. 2004) with redshifts corresponding to  $H\alpha$  emitters,  $[O III]$  emitters,  $H\beta$  emitters, and  $[O II]$  emitters are shown as red, green, light blue, and blue open squares, respectively.

the contribution of these lines. The flux of the  $H\alpha$  emission line is also affected by the internal extinction. Therefore, we have to correct the contamination of the  $[N II] \lambda\lambda 6548, 6583$  emission and the internal extinction  $A_{H\alpha}$ . Although several correction methods have been proposed (e.g., Kennicutt 1992a, Gallego et al. 1997, Tresse et al. 1999, and Helmboldt et al. 2004 for  $[N II]$

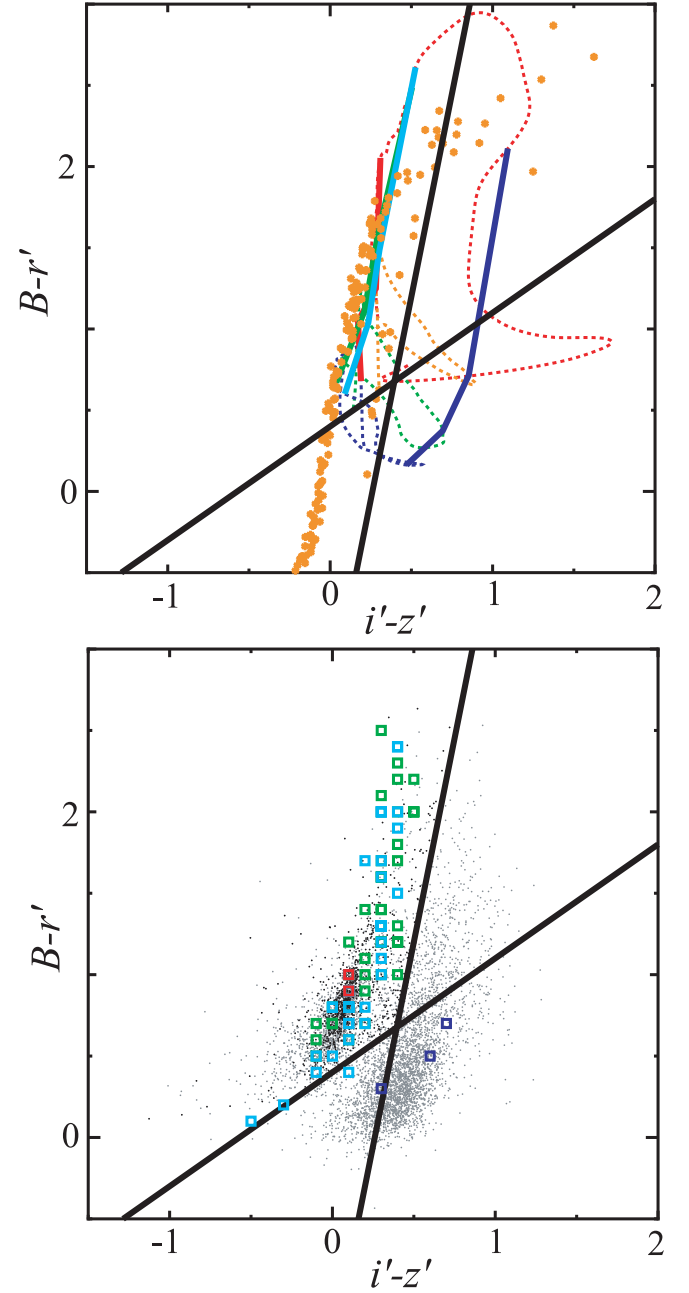


FIG. 3.—Diagrams of  $B - r'$  vs.  $i' - z'$ . *Top*: Colors of model galaxies (CWW) from  $z = 0$  to  $z = 3$  are shown with dotted lines: red, orange, green, and blue lines show the loci of E, Sbc, Scd, and Irr galaxies, respectively. Colors of  $z = 0.24, 0.64, 0.68$ , and  $1.18$  (for  $H\alpha$ ,  $[O III]$ ,  $H\beta$ , and  $[O II]$  emitters, respectively) are shown with red, green, light blue, and blue lines, respectively. Orange asterisks show the star of Gunn & Stryker (1983). *Bottom*: Plot of  $B - r'$  vs.  $i' - z'$  for the 6176 sources found with emitter selection criteria (black dots). In this diagram,  $H\alpha$  emitters are located above both of the black lines, adopted by us as one of the criteria for the selection of  $H\alpha$  emitters. The 980  $H\alpha$  emitters are shown as black dots, and other emission-line galaxy candidates are shown as gray dots. Galaxies in GOODS-N (Cowie et al. 2004) with redshifts corresponding to  $H\alpha$  emitters,  $[O III]$  emitters,  $H\beta$  emitters, and  $[O II]$  emitters are shown as red, green, light blue, and blue open squares, respectively.

contamination; Kennicutt 1983b, 1998, Niklas et al. 1997, Hopkins et al. 2001, and Afonso et al. 2003 for  $A_{H\alpha}$ ), there are few studies that give both corrections based on a single sample of galaxies. Helmboldt et al. (2004) derived the relation between  $[N II]/H\alpha$  and  $M_R$  and that between  $A_{H\alpha}$  and  $M_R$  based on the data of the Nearby Field Galaxy Survey (Jansen et al. 2000a, 2000b). We



TABLE 1  
A LIST OF H $\alpha$  EMITTER CANDIDATES

Number	ID	R.A. (J2000.0) (deg)	Decl. (J2000.0) (deg)	$i'$ (mag)	$z'$ (mag)	NB816 (mag)	$iz$ (mag)	$iz - \text{NB816}$ (mag)	$\log F_L$ (ergs s $^{-1}$ cm $^{-2}$ )	$\log F_{\text{cor}}$ (ergs s $^{-1}$ cm $^{-2}$ )	$\log L(\text{H}\alpha)$ (ergs s $^{-1}$ )	EW $_{\text{obs}}$ ( $\text{\AA}$ )
1.....	58612	150.72533	1.611834	20.99	20.92	20.86	20.96	0.10	-16.11	-15.81	40.44	12
2.....	62649	150.67970	1.594458	20.89	20.64	20.64	20.78	0.13	-15.88	-15.57	40.67	17
3.....	101151	150.46013	1.600051	21.05	21.05	20.93	21.05	0.12	-16.05	-15.76	40.49	14
4.....	135016	150.33841	1.622284	22.98	22.58	22.70	22.79	0.09	-16.87	-16.67	39.58	11
5.....	137365	150.32673	1.605641	23.01	22.91	22.84	22.96	0.13	-16.78	-16.58	39.67	16

NOTE.—Table 1 is available in its entirety in the electronic edition of the *Supplement*. A portion is shown here for guidance regarding its form and content.

therefore adopt their relations to correct the [N II] contamination and  $A_{\text{H}\alpha}$ . After correcting to the AB magnitude system (Meurer et al. 2006), the relation between [N II]/H $\alpha$  and  $M_R$  is

$$\log w_{6583} = -0.13M_R - 3.30, \quad (9)$$

where

$$w_{6583} \equiv \frac{F_{[\text{N II}]6583 \text{ \AA}}}{F_{\text{H}\alpha}}, \quad (10)$$

and that between  $A_{\text{H}\alpha}$  and  $M_R$  is

$$\log A_{\text{H}\alpha} = -0.12M_R - 2.47. \quad (11)$$

To derive  $M_R$  used in equations (9) and (11) for each galaxy, we assume that the redshift of the galaxy is  $z = 0.242$ . We have also calculated the  $k$ -correction using the average SED of the Coleman et al. (1980) Sbc and Irr. Taking account of the luminosity distance and  $k$ -correction (average value of Scd and Irr),  $M_R$  is calculated from  $r'$ -band total magnitude,  $r'$ , as  $M_R = r' - 40.90$ .

In addition to the above corrections, we also apply a statistical correction (21%; the average value of flux decrease due to the filter transmission) to the measured flux because the filter transmission function is not square in shape (Fujita et al. 2003). Note that this value is slightly different from the value (28%) used in Fujita et al. (2003). Our new value is re-estimated by using the latest filter response function. The H $\alpha$  flux is given by

$$F_{\text{cor}}(\text{H}\alpha) = F_L \frac{f(\text{H}\alpha)}{f(\text{H}\alpha) + f([\text{N II}])} \times 10^{0.4A_{\text{H}\alpha}} \times 1.21. \quad (12)$$

Finally, the H $\alpha$  luminosity is estimated by  $L(\text{H}\alpha) = 4\pi d_L^2 F_{\text{cor}}(\text{H}\alpha)$ . In this procedure, we assume that all the H $\alpha$  emitters are located at  $z = 0.242$ , which is the redshift corresponding to the central wavelength of our NB816 filter. Therefore, the luminosity distance is set to be  $d_L = 1213$  Mpc.

We summarize the total magnitude of  $i'$ ,  $z'$ , NB816, and  $iz$  and the color excess of  $iz - \text{NB816}$  for our H $\alpha$  emission-line galaxy candidates in Table 1. Table 1 also includes  $\log F_L$ ,  $\log F_{\text{cor}}(\text{H}\alpha)$ , and  $\log L(\text{H}\alpha)$ .

#### 4. DISCUSSION

##### 4.1. Luminosity Function of H $\alpha$ Emitters

Figure 4 shows the H $\alpha$  luminosity function (LF) at  $z \approx 0.24$  for our H $\alpha$  emitter sample. The H $\alpha$  LF is constructed by the relation

$$\Phi(\log L_i) = \frac{1}{\Delta \log L} \sum_j \frac{1}{V_j}, \quad (13)$$

with

$$|\log L_j - \log L_i| < \frac{1}{2} \Delta \log L, \quad (14)$$

where  $V_j$  is the volume of the narrowband slice in the range of redshift covered by the filter. We have used  $\Delta \log L(\text{H}\alpha) = 0.2$ . If the shape of the filter response is square, our survey volume is  $3.1 \times 10^4$  Mpc $^3$ . However, the effective survey volume is affected by the shape of the filter transmission curve. For example, since the transmission at 8092  $\text{\AA}$  is one-half of the peak value, the color excess,  $iz - \text{NB816}$ , of an H $\alpha$  emitter at  $z = 0.233$  with  $\text{EW}(\text{H}\alpha + [\text{N II}]) = 12$   $\text{\AA}$  is observed as 0.05, which does not satisfy our selection criterion,  $iz - \text{NB816} > 0.1$ . Taking account of the filter shape in the computation of the volume, the correction can be as large as 23% for the faintest galaxies. Adopting the Schechter function form (Schechter 1976), we obtain the following best-fit parameters for our H $\alpha$  emitters with  $L(\text{H}\alpha) > 10^{39.8}$  ergs s $^{-1}$ :  $\alpha = -1.35^{+0.11}_{-0.13}$ ,  $\log \phi_* = -2.65^{+0.27}_{-0.38}$ , and  $\log L_*(\text{ergs s}^{-1}) = 41.94^{+0.38}_{-0.23}$  (black solid line).

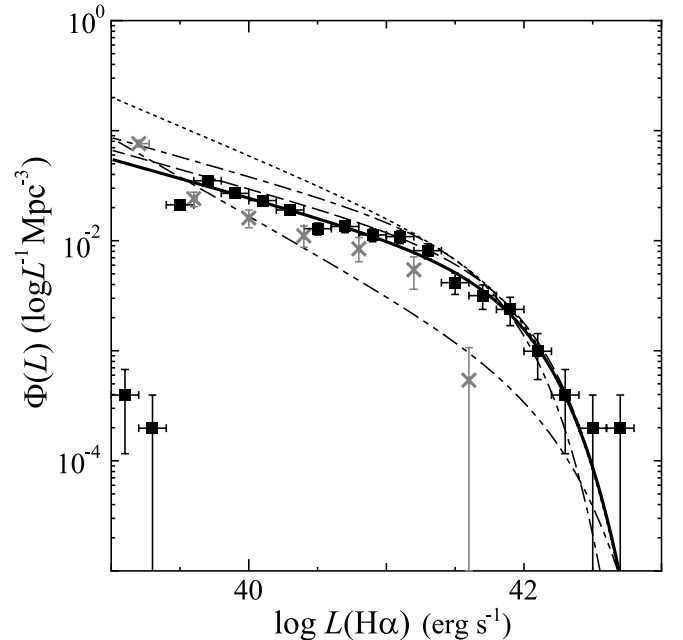


FIG. 4.—Our H $\alpha$  luminosity function (filled squares and thick solid line) and H $\alpha$  luminosity functions from previous works. The Tresse & Maddox (1998) H $\alpha$  luminosity function at  $z \leq 0.3$  is shown by the dashed line. The H $\alpha$  luminosity functions derived by Fujita et al. (2003), Hippelein et al. (2003), and Ly et al. (2007) are shown by the dotted line, the dot-dashed line, and dashed and double-dotted line, respectively. Data points of the Ly et al. (2007) H $\alpha$  LF are shown as gray crosses.

Together with our H $\alpha$  LF, Figure 4 shows H $\alpha$  LFs of previous studies in which H $\alpha$  emitters at  $z < 0.3$  are investigated: Tresse & Maddox (1998, which is characterized by  $\alpha = -1.35$ ,  $\phi_* = 10^{-2.56} \text{ Mpc}^{-3}$ , and  $L_* = 10^{41.92} \text{ ergs s}^{-1}$ ; note that these parameters were converted by Hopkins [2004] to those of our adopted cosmology), Fujita et al. (2003), Hippelein et al. (2003) and Ly et al. (2007). Fujita et al. (2003), Ly et al. (2007), and this work are based on the NB816 imaging obtained with the Subaru Telescope. Tresse & Maddox (1998) is based on the Canada-France Redshift Survey (CFRS), and Hippelein et al. (2003) is based on the Calar Alto Deep Imaging Survey (CADIS).

First, we compare our H $\alpha$  LF with that derived by Ly et al. (2007). Their best-fit Schechter function parameters ( $\alpha = -1.71$ ,  $\log \phi_* = -3.7$ ,  $\log L_* = 42.2$ ) are quite different from those of our H $\alpha$  LF. However, we note that the data points between  $\log L(\text{H}\alpha) \sim 39.5$  and  $\sim 41.0$ , shown in Figure 10b of Ly et al. (2007), are quite similar to our results (Fig. 4). We therefore consider that the H $\alpha$  LF of Ly et al. (2007) itself is basically consistent with ours except for the brightest point. The difference between our Schechter parameters and those of Ly et al. may arise from the data points of the brightest and the faintest ones, especially the brightest one. Since the field of view of the COSMOS is about an order of magnitude wider than that of the SDF, we consider that our H $\alpha$  LF is more accurate than that determined by Ly et al. (2007) at the bright end.

Second, we compare our H $\alpha$  LF with the other H $\alpha$  LFs. Although our H $\alpha$  LF is similar to those of Tresse & Maddox (1998) and Hippelein et al. (2003), the H $\alpha$  LF of Fujita et al. (2003) shows a steeper faint-end slope and a higher number density for the same luminosity. These differences may be attributed to the following different source selection procedures: (1) Fujita et al. (2003) used their NB816-selected galaxies, while we used  $i'$ -selected galaxies, Tresse & Maddox (1998) used  $I$ -selected Canada-France Redshift Survey (CFRS) galaxies, and Hippelein et al. (2003) used Fabry-Perot images for preselection of emission-line galaxies. As Fujita et al. (2003) demonstrated, samples based on a broadband selected catalog are biased against galaxies with faint continuum. (2) Fujita et al. (2003) used their  $B - R_C$  versus  $R_C - I_C$  color-color diagram to isolate H $\alpha$  emitters from other low- $z$  emitters at different redshifts. However, we find that there are possible contaminations of [O III] emitters if one uses the  $B - R_C$  versus  $R_C - I_C$  diagram, because of the small difference between H $\alpha$  and [O III] emitters on that color-color diagram. On the other hand, we used  $B - V$  versus  $V - r'$  to isolate H $\alpha$  emitters from [O III] emitters. Due to the large separation between H $\alpha$  emitters and [O III] emitters on the  $B - V$  versus  $V - r'$  diagram, we can reduce the contamination of [O III] emitters. (3) Fujita et al. (2003) used the population synthesis model GISEL96 (Bruzual & Charlot 1993) to determine the criteria for selecting H $\alpha$  emitters. To check the validity of the criterion, we compare colors of GOODS-N galaxies at  $z \sim 0.24, 0.63, 0.68$ , and  $1.19$  with model colors at corresponding redshifts based on GISEL96 (Fig. 5). Unfortunately, the predicted colors are slightly different from those of observed galaxies. We therefore redetermined the selection criteria using the SED of Coleman et al. (1980) as

$$(B - R_C) > 2.5(R_C - I_C) + 0.2.$$

If we adopt this revised criterion, the number of H $\alpha$  emitters in Fujita et al. (2003) is reduced by about 20% (Fig. 5). This is one reason why the number density of H $\alpha$  emitters in Fujita et al. (2003) is higher than other surveys. Recently, Ly et al. (2007) pointed out that the fraction of [O III] emitters in the H $\alpha$  emitter

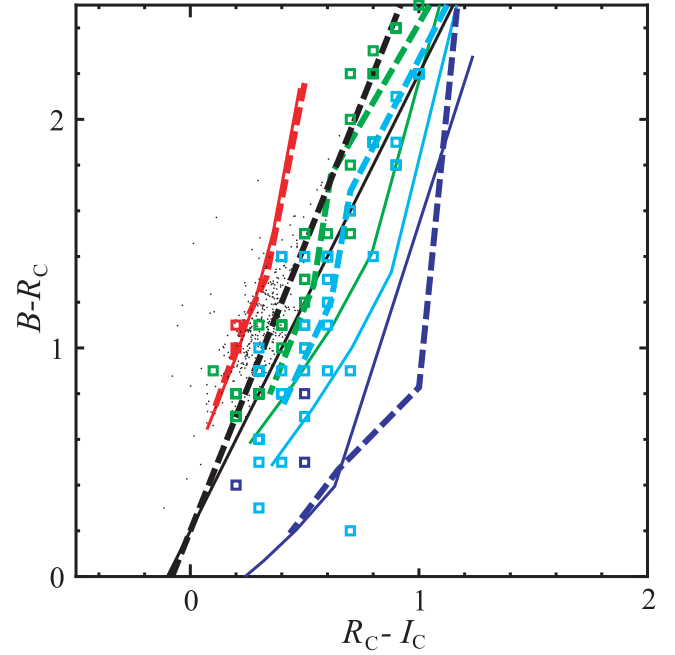


FIG. 5.— $B - R_C$  vs.  $R_C - I_C$  color-color diagram of model galaxies. Colors of  $z = 0.24, 0.64, 0.68$ , and  $1.18$  (for H $\alpha$ , [O III], H $\beta$ , and [O II] emitters, respectively) are shown with red, green, light blue, and blue lines, respectively. The loci calculated by using GISEL96 (Bruzual & Charlot 1993) are shown by solid lines, and those calculated by using CWW are shown by dashed lines. Galaxies in GOODS-N (Cowie et al. 2004) with redshifts corresponding to H $\alpha$  emitters, [O III] emitters, H $\beta$  emitters, and [O II] emitters are shown as red, green, light blue, and blue open squares, respectively. Fujita et al. (2003) selected galaxies above the black solid line as H $\alpha$  emitter candidates. If we reselect H $\alpha$  emitter candidates as sources above the black dashed line, some of the H $\alpha$  emitter candidates (black dots) do not satisfy the new criterion.

sample of Fujita et al. (2003) may be about 50% using the Hawaii HDF-N sources with redshifts observed as NB816-excess objects. The H $\alpha$  LF of Fujita et al. (2003) reduced by 50% appears to be quite similar to our H $\alpha$  LF.

#### 4.2. Luminosity Density and Star Formation Rate Density

By integrating the luminosity function, i.e.,

$$\mathcal{L}(\text{H}\alpha) = \int_0^\infty \Phi(L) dL = \Gamma(\alpha + 2) \phi_* L_*, \quad (15)$$

we obtain a total H $\alpha$  luminosity density of  $2.7^{+0.7}_{-0.6} \times 10^{39} \text{ ergs s}^{-1} \text{ Mpc}^{-3}$  at  $z \approx 0.24$  from our best-fit LF. The star formation rate is estimated from the H $\alpha$  luminosity using the relation  $\text{SFR} = 7.9 \times 10^{-42} L(\text{H}\alpha) M_\odot \text{ yr}^{-1}$ , where  $L(\text{H}\alpha)$  is in units of  $\text{ergs s}^{-1}$  (Kennicutt 1998). Using this relation, the H $\alpha$  luminosity density can be translated into the SFR density of  $\rho_{\text{SFR}} \simeq 2.1^{+1.0}_{-0.4} \times 10^{-2} M_\odot \text{ yr}^{-1} \text{ Mpc}^{-3}$ .

However, not all the H $\alpha$  luminosity is produced by star formation, because active galactic nuclei (AGNs) can also contribute to the H $\alpha$  luminosity. For example, previous studies obtained the following estimates: 8%–17% of the galaxies in the CFRS low- $z$  sample (Tresse et al. 1996), 8% in the Universidad Complutense de Madrid (UCM) survey of local H $\alpha$  emission line galaxies (Gallego et al. 1995), and 17%–28% in the 15R survey (Carter et al. 2001). Recently, Hao et al. (2005) obtained an H $\alpha$  luminosity function of AGNs based on the sample of the Sloan Digital Sky Survey within a redshift range of  $0 < z < 0.15$ . The H $\alpha$  luminosity density calculated from the Schechter function parameters that are shown in the paper is  $1.1 \times 10^{38} \text{ ergs s}^{-1} \text{ Mpc}^{-3}$

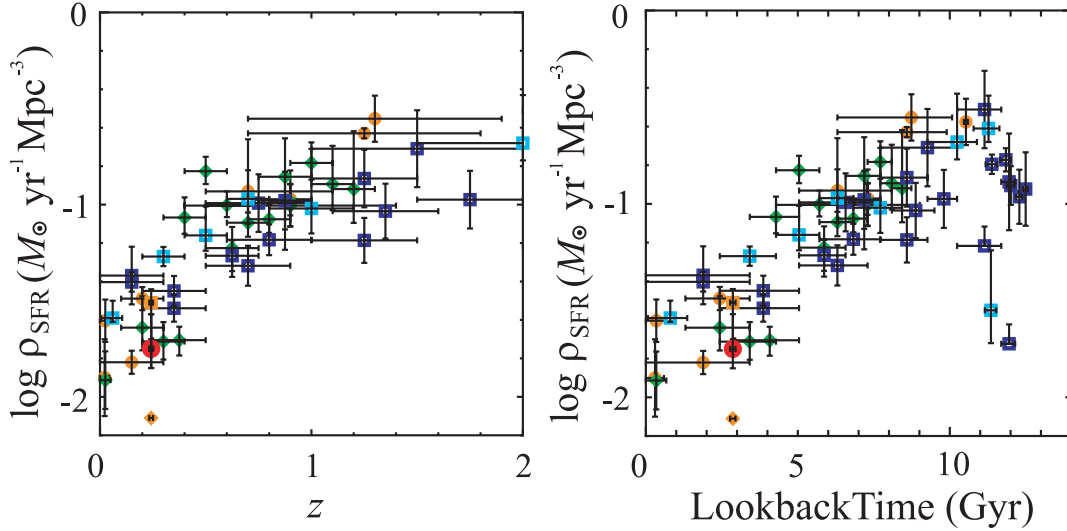


FIG. 6.— Star formation rate density (SFRD) at  $z \approx 0.24$  derived from this study (large red filled circle) shown together with the previous investigations compiled by Hopkins (2004). SFRDs estimated from  $H\alpha$ ,  $[O II]$ , and UV continuum are shown as orange open circles (Pérez-González et al. 2003; Tresse et al. 2002; Moorwood et al. 2000; Hopkins et al. 2000; Glazebrook et al. 1999; Yan et al. 1999; Tresse & Maddox 1998; Gallego et al. 1995), green open diamonds (Teplitz et al. 2003; Gallego et al. 2002; Hogg et al. 1998; Hammer et al. 1997), and blue squares (Wilson et al. 2002; Massarotti et al. 2001; Sullivan et al. 2000; Cowie et al. 1999; Treyer et al. 1998; Connolly et al. 1997; Lilly et al. 1996). The light blue open squares show SFRDs based on the UV luminosity density by Schiminovich et al. (2005), assuming  $A_{FUV} = 1.8$ . An orange open square and an orange open diamond show SFRDs at  $z \approx 0.24$  derived by Fujita et al. (2003) and Ly et al. (2007), respectively. In the left panel we show the evolution of SFRD as a function of redshift, and in the right panel we show it as a function of look-back time.

(with no reddening correction). Taking account of the reddening correction and the  $H\alpha$  luminosity density radiated from star-forming galaxies (Gallego et al. 1995), the fraction of AGN contribution to the total  $H\alpha$  luminosity density is about 15% in the local universe. If we assume that 15% of the  $H\alpha$  luminosity density is radiated from AGNs, the corrected SFRD is  $1.8^{+0.7}_{-0.4} \times 10^{-2} M_{\odot} \text{ yr}^{-1} \text{ Mpc}^{-3}$ .

We note here that the error for  $\rho_{\text{SFR}}$  [and  $\mathcal{L}(H\alpha)$ ] is probably underestimated, since it does not include the effects of different correction methods and selection biases. For example, adopting the different relation for correcting  $A_{H\alpha}$  may cause a different value of SFRD.

We compare our result with the previous investigations compiled by Hopkins (2004) in Figure 6. We also show the evolution of SFRD derived from the observation of *GALEX* with mean attenuation of  $A_{\text{UV}}^{\text{meas}} = 1.8$ , evaluated from the FUV slope  $\beta$  ( $f_{\lambda} \propto \lambda^{\beta}$ ) and the relation of  $A_{\text{FUV}} = 4.43 + 1.99\beta$ . If we adopt the more representative value  $A_{\text{UV}}^{\text{min}} = 1$  (Schiminovich et al. 2005) determined by using the  $F_{\text{dust}}/F_{\text{UV}}$  ratio (Buat et al. 2005), their SFRD becomes smaller by a factor of 2, being similar to our SFRD.

The left panel of Figure 6 shows the evolution of the SFRD as a function of redshift from  $z = 0$  to  $z = 2$ . The right panel of Figure 6 shows that as a function of the look-back time. It clearly shows that SFRD monotonically decreasing for 10 Gyr with increasing cosmic time. We note that the error of SFRD of our evaluation includes only random error, since we adopt the same assumptions as those in Hopkins (2004).

Our SFRD evaluated above seems roughly consistent with but slightly smaller than the previous evaluations, e.g., those of Tresse & Maddox (1998) and Fujita et al. (2003). Since we select emission-line galaxies with  $\text{EW}(H\alpha + [N II])_{\text{obs}} > 12 \text{ \AA}$ , our sample is considered to be biased against star-forming galaxies with small specific SFR, which is defined as the ratio of SFR to stellar mass of galaxy. Since our criterion is similar to that of Tresse & Maddox (1998) and the same as that of Fujita et al. (2003), we consider that the difference between our survey and theirs is not

caused by the different criteria of  $\text{EW}(H\alpha + [N II])_{\text{obs}}$ . As we mentioned in § 4.1, the SFRD of Fujita et al. (2003) was overestimated because of the contamination of  $[O III]$  emitters. On the other hand, the difference between Tresse & Maddox (1998) and our work seems to be real; e.g., the cosmic variance.

We discuss further the effect of the selection criterion of  $\text{EW}(H\alpha + [N II])_{\text{obs}} > 12 \text{ \AA}$  on the evaluation of SFRD. Being different from the previous  $H\alpha$  emission-line galaxy surveys using the objective prism, the fraction of galaxies having  $\text{EW}(H\alpha) > 50 \text{ \AA}$  is 12% in our sample, which is similar to or less than the value of the local universe (15%–20%: Heckman 1998) and SINGG SR1 (14.5%: Hanish et al. 2006). On the other hand, the fractions of the galaxies with  $\text{EW}(H\alpha) > 50 \text{ \AA}$  are 42% and 35% in the KPNO International Spectroscopic Survey (KISS; Gronwall et al. 2004) and UCM objective-prism surveys, respectively. Our sample seems to be not strongly biased toward galaxies with high equivalent width. Hanish et al. (2006) showed that 4.5% of the  $H\alpha$  luminosity density comes from galaxies with  $\text{EW}(H\alpha) < 10 \text{ \AA}$  in local universe. If the fraction (4.5%) is valid for the star-forming galaxies at  $z \approx 0.24$ , our estimate of SFRD would be about 5% smaller than the true SFRD.

#### 4.3. Spatial Distribution and Angular Two-Point Correlation Function

Figure 7 shows the spatial distribution of our 980  $H\alpha$  emitter candidates. There are some clustering regions over the field. To discuss the clustering properties more quantitatively, we derive the angular two-point correlation function (ACF),  $w(\theta)$ , using the estimator defined by Landy & Szalay (1993):

$$w(\theta) = \frac{DD(\theta) - 2DR(\theta) + RR(\theta)}{RR(\theta)}, \quad (16)$$

where  $DD(\theta)$ ,  $DR(\theta)$ , and  $RR(\theta)$  are normalized numbers of galaxy-galaxy, galaxy-random, and random-random pairs, respectively. The random sample consists of 100,000 sources with the same geometrical constraints as the galaxy sample. Figure 4

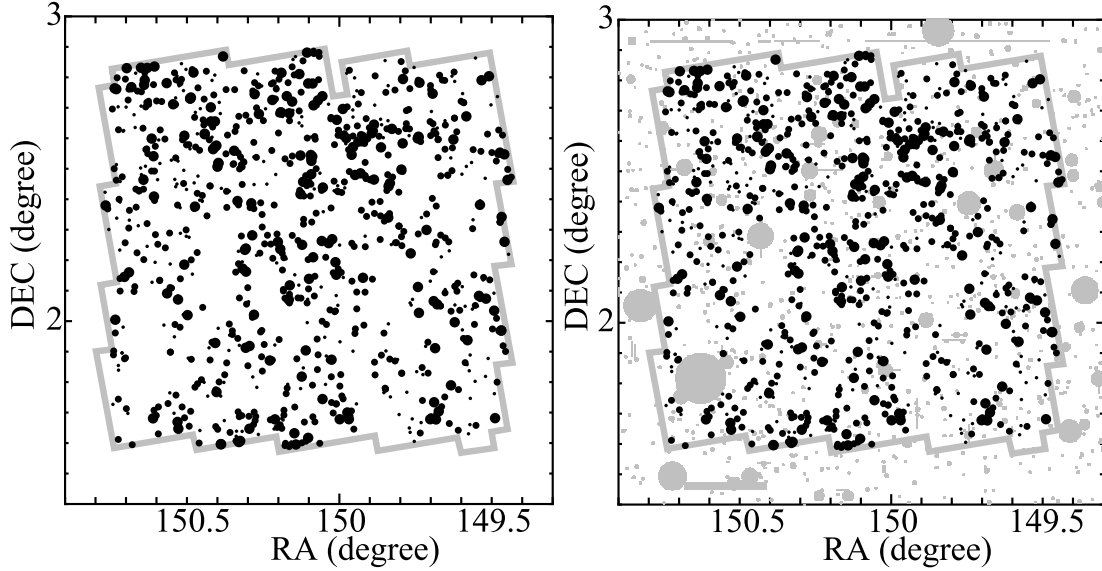


FIG. 7.—Spatial distributions of our H $\alpha$  emitter candidates (*black filled circles and black dots*). Gray open squares in both panels show our survey area. The shaded regions in the right panel show the areas masked out for the detection. We show the luminous H $\alpha$  emitters [ $\log L(\text{H}\alpha)(\text{ergs s}^{-1}) > 40.94$ ] as large filled circles and the faint H $\alpha$  emitters [ $39.8 < \log L(\text{H}\alpha)(\text{ergs s}^{-1}) \leq 40.94$ ] as small filled circles. H $\alpha$  emitters with  $\log L(\text{H}\alpha)(\text{ergs s}^{-1}) \leq 39.8$  are shown as black dots.

demonstrates that our H $\alpha$  emitter sample is quite incomplete for  $\log L(\text{H}\alpha)(\text{ergs s}^{-1}) < 39.8$ . We therefore show the ACF for 693 H $\alpha$  emitter candidates with  $\log L(\text{H}\alpha)(\text{ergs s}^{-1}) > 39.8$  in Figure 8. The ACF is fit well by a power law,  $w(\theta) = 0.013^{+0.002}_{-0.001}\theta^{-0.88 \pm 0.03}$ . Recently, the departure from a power law of the correlation function was reported (Zehavi et al. 2004; Ouchi et al. 2005). Such a departure may be interpreted as the transi-

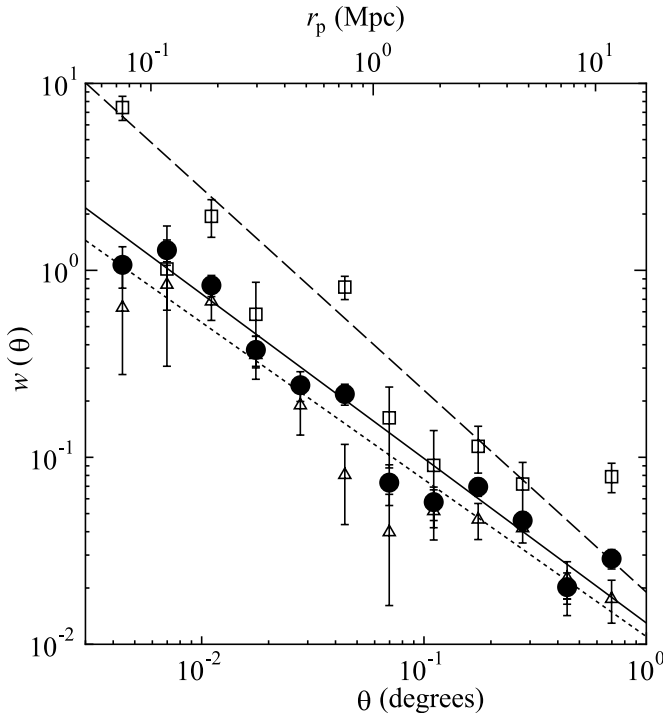


FIG. 8.—Angular two-point correlation function of all H $\alpha$  emitter candidates (*filled circles*), bright H $\alpha$  emitter candidates ( $\log L(\text{H}\alpha)(\text{ergs s}^{-1}) > 40.94$ ; *open squares*), and faint H $\alpha$  emitter candidates ( $39.8 < \log L(\text{H}\alpha)(\text{ergs s}^{-1}) \leq 40.94$ ; *open triangles*). Solid line shows the relation of  $w(\theta) = 0.013\theta^{-0.88}$ . Dashed line shows the best-fitting power law for bright ones,  $w(\theta) = 0.019\theta^{-1.08}$ , and dotted line shows that for faint ones,  $w(\theta) = 0.011\theta^{-0.84}$ .

tion from a large-scale regime, where a pair of galaxies resides in separate halos, to a small-scale regime, where a pair of galaxies resides within the same halo. We find no evidence for such a departure in our result. We, however, consider that the number of our sample is too small to discuss this problem.

For Lyman-break galaxies, brighter galaxies (with a larger star formation rate) tend to show more clustered structures than faint ones (with a smaller star formation rate; e.g., Ouchi et al. 2004; Kashikawa 2006). We also show the ACF of H $\alpha$  emitters with larger H $\alpha$  luminosity [ $\log L(\text{H}\alpha)(\text{ergs s}^{-1}) > 40.94 = \log(0.1L_*)$ ] and those with lower H $\alpha$  luminosity [ $39.8 < \log L(\text{H}\alpha)(\text{ergs s}^{-1}) \leq 40.94$ ] in Figure 8. Both ACFs are well fit with a power-law form:  $w(\theta) = 0.019^{+0.004}_{-0.004}\theta^{-1.08 \pm 0.05}$  for objects with  $\log L(\text{H}\alpha)(\text{ergs s}^{-1}) > 40.94$ , while  $w(\theta) = 0.011^{+0.002}_{-0.002}\theta^{-0.84 \pm 0.05}$  for objects with  $39.8 < \log L(\text{H}\alpha)(\text{ergs s}^{-1}) \leq 40.94$ , respectively. We conclude that galaxies with a higher star formation rate are more strongly clustered than ones with a lower star formation rate. This fact is interpreted as that galaxies with a higher star formation rate reside in more massive dark matter halos, which are more clustered in the hierarchical structure formation scenario.

It is useful to evaluate the correlation length  $r_0$  of the two-point correlation function  $\xi(r) = (r/r_0)^{-\gamma}$ . A correlation length is derived from the ACF through Limber's equation (e.g., Peebles 1980). Assuming that the redshift distribution of H $\alpha$  emitters is a top hat shape of  $z = 0.242 \pm 0.009$ , we obtain the correlation length of  $r_0 = 1.9$  Mpc. Therefore, the two-point correlation function for all H $\alpha$  emitters is written as  $\xi(r) = (r/1.9 \text{ Mpc})^{-1.88}$ . The correlation length of H $\alpha$  emitters with  $\log L(\text{H}\alpha)(\text{ergs s}^{-1}) > 40.94$  is 2.9 Mpc, while that of H $\alpha$  emitters with  $39.8 < \log L(\text{H}\alpha)(\text{ergs s}^{-1}) \leq 40.94$  is 1.6 Mpc. These values are smaller than those evaluated for nearby  $L_*$  galaxies ( $\sim 7$  Mpc; Norberg et al. 2001; Zehavi et al. 2005) and  $z \sim 1$  galaxies ( $\sim 4-5$  Mpc; Coil et al. 2004).

It is known that the correlation length is smaller for fainter galaxies in the nearby (Norberg et al. 2001; Zehavi et al. 2005) and  $z \sim 1$  universe (Coil et al. 2006). Figure 9 shows the relation between the  $L(\text{H}\alpha)$ - and  $R_C$ -band absolute magnitude  $M_R$  for our sample. Our sample includes many faint ( $M_R > -18$ ) galaxies. However, the correlation length for galaxies with  $-18 < M_r < -17$

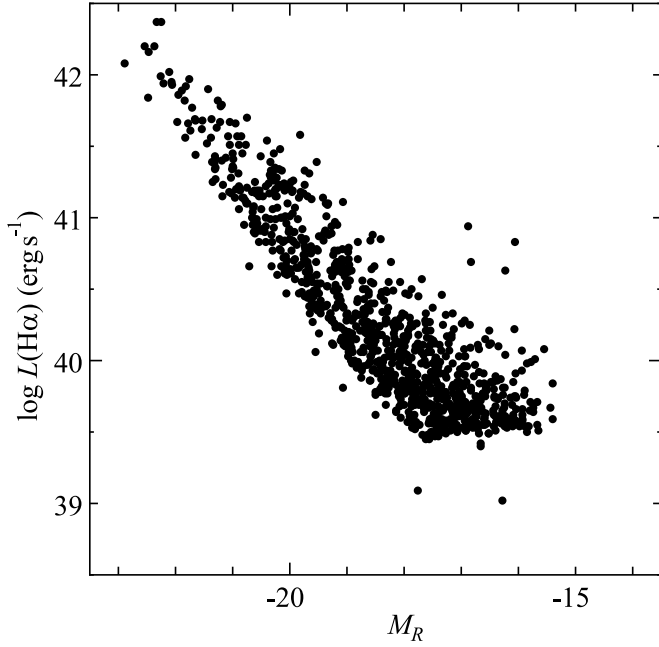


FIG. 9.—Relation between  $H\alpha$  luminosities and  $R$ -band absolute magnitudes for our  $H\alpha$  emitters.

(3.8 Mpc; Zehavi et al. 2005) is still larger than that of our sample. This discrepancy may imply a weak clustering of emission-line galaxies.

## 5. SUMMARY

We have performed the  $H\alpha$  emitter survey in the *HST* COSMOS 2 square degree field using the COSMOS official photometric catalog. Our results and conclusions are summarized as follows:

1. We found 980  $H\alpha$  emission-line galaxy candidates using the narrowband imaging method. The  $H\alpha$  luminosity function is

well fit by a Schechter function with  $\alpha = -1.35^{+0.11}_{-0.13}$ ,  $\log \phi_* = -2.65^{+0.27}_{-0.38}$ , and  $\log L_*(\text{ergs s}^{-1}) = 41.94^{+0.38}_{-0.23}$ . Using the parameter set of the Schechter function, the  $H\alpha$  luminosity density is evaluated as  $2.7^{+0.7}_{-0.6} \times 10^{39} \text{ ergs s}^{-1} \text{ Mpc}^{-3}$ . If we adopt the AGN contribution to the  $H\alpha$  luminosity density to be 15%, we obtain a star formation rate density of  $1.8^{+0.7}_{-0.4} \times 10^{-2} M_\odot \text{ yr}^{-1} \text{ Mpc}^{-3}$ . This error includes only random error. Our result supports the strong increase in SFRD from  $z = 0$  to  $z = 1$ .

2. We studied the clustering properties of  $H\alpha$  emitters at  $z \sim 0.24$ . The two-point correlation function is well fit by a power law,  $w(\theta) = 0.013^{+0.002}_{-0.001} \theta^{-0.88 \pm 0.03}$ , which leads to the correlation function of  $(r/1.9 \text{ Mpc})^{-1.88}$ . We cannot find the departure from a power law, which was recently found in both low- and high- $z$  galaxies. Although the power of  $-1.88$  is consistent with the power for nearby galaxies, the derived correlation length of  $r_0 = 1.9 \text{ Mpc}$  is smaller than that for nearby galaxies with the same optical luminosity range. This discrepancy may imply a weak clustering of emission-line galaxies. The galaxies with higher SFR are more strongly clustered than those with lower SFR. Taking account of the fact that the SFR of a luminous galaxy is higher than that of a faint galaxy, this result is consistent with the previously known fact that luminous galaxies are more strongly clustering.

The *HST* COSMOS Treasury program was supported through NASA grant HST-GO-09822. We greatly acknowledge the contributions of the entire COSMOS collaboration consisting of more than 70 scientists. The COSMOS science meeting in 2005 May was supported by in part by the NSF through grant OISE-0456439. We would also like to thank the Subaru Telescope staff for their invaluable help. This work was financially supported in part by the JSPS (nos. 15340059 and 17253001). S. S. S. and T. N. are JSPS fellows.

## REFERENCES

- Afonso, J., Hopkins, A., Mobasher, B., & Almeida, C. 2003, *ApJ*, 597, 269  
 Bell, E. F. 2003, *ApJ*, 586, 794  
 Bertin, E., & Arnouts, S. 1996, *A&AS*, 117, 393  
 Bouwens, R. J., & Illingworth, G. D. 2006, *Nature*, 443, 189  
 Bruzual, A., G., & Charlot, S. 1993, *ApJ*, 405, 538  
 Buat, V., et al. 2005, *ApJ*, 619, L51  
 Capak, P., et al. 2007, *ApJS*, 172, 99  
 Carter, B. J., Fabricant, D. G., Geller, M. J., Kurtz, M. J., & McLean, B. 2001, *ApJ*, 559, 606  
 Charlot, S., Kauffmann, G., Longhetti, M., Tresse, L., White, S. D. M., Maddox, S. J., & Fall, S. M. 2002, *MNRAS*, 330, 876  
 Charlot, S., & Longhetti, M. 2001, *MNRAS*, 323, 887  
 Coil, A. L., et al. 2004, *ApJ*, 609, 525  
 ———. 2006, *ApJ*, 644, 671  
 Coleman, G. D., Wu, C.-C., & Weedman, D. W. 1980, *ApJS*, 43, 393  
 Condon, J. J. 1992, *ARA&A*, 30, 575  
 Connolly, A. J., Szalay, A. S., Dickinson, M., SubbaRao, M. U., & Brunner, R. J. 1997, *ApJ*, 486, L11  
 Cowie, L. L., Barger, A. J., Hu, E. M., Capak, P., & Songaila, A. 2004, *AJ*, 127, 3137  
 Cowie, L. L., Songaila, A., & Barger, A. J. 1999, *AJ*, 118, 603  
 Fujita, S. S., et al. 2003, *ApJ*, 586, L115  
 Gallego, J., García-Dabó, C. E., Zamorano, J., Aragón-Salamanca, A., & Rego, M. 2002, *ApJ*, 570, L1  
 Gallego, J., Zamorano, J., Aragón-Salamanca, A., & Rego, M. 1995, *ApJ*, 455, L1; Erratum 1996, *ApJ*, 459, L43  
 Gallego, J., Zamorano, J., Rego, M., & Vitores, A. G. 1997, *ApJ*, 475, 502  
 Gavazzi, G., Cocito, A., & Vettolani, G. 1986, *ApJ*, 305, L15  
 Giavalisco, M., et al. 2004, *ApJ*, 600, L103  
 Glazebrook, K., Blake, C., Economou, F., Lilly, S., & Colless, M. 1999, *MNRAS*, 306, 843  
 Gronwall, C., Salzer, J. J., Sarajedini, V. L., Jangren, A., Chomiuk, L., Moody, J. W., Frattare, L. M., & Boroson, T. A. 2004, *AJ*, 127, 1943  
 Gunn, J. E., & Stryker, L. L. 1983, *ApJS*, 52, 121  
 Hammer, F., et al. 1997, *ApJ*, 481, 49  
 Hanish, D. J., et al. 2006, *ApJ*, 649, 150  
 Hao, L., et al. 2005, *AJ*, 129, 1795  
 Heckman, T., 1998, in *ASP Conf. Ser.* 148, *Origins*, ed. C. E. Woodward, J. M. Shull, & H. A. Thronson (San Francisco: ASP), 127  
 Helmboldt, J. F., Walterbos, R. A. M., Bothun, G. D., O’Neil, K., & de Blok, W. J. G. 2004, *ApJ*, 613, 914  
 Hippelein, H., et al. 2003, *A&A*, 402, 65  
 Hogg, D. W., Cohen, J. G., Blandford, R., & Pahre, M. A. 1998, *ApJ*, 504, 622  
 Hopkins, A. M. 2004, *ApJ*, 615, 209  
 Hopkins, A. M., Connolly, A. J., Haarsma, D. B., & Cram, L. E. 2001, *AJ*, 122, 288  
 Hopkins, A. M., Connolly, A. J., & Szalay, A. S. 2000, *AJ*, 120, 2843  
 Hopkins, A. M., et al. 2003, *ApJ*, 599, 971  
 Iye, M., et al. 2004, *PASJ*, 56, 381  
 Jansen, R. A., Fabricant, D., Franx, M., & Caldwell, N. 2000a, *ApJS*, 126, 331  
 Jansen, R. A., Franx, M., Fabricant, D., & Caldwell, N. 2000b, *ApJS*, 126, 271  
 Kaifu, N., et al. 2000, *PASJ*, 52, 1  
 Kashikawa, N. 2006, *ApJ*, 637, 631  
 Kennicutt, R. 1983a, *A&A*, 120, 219  
 Kennicutt, R. C., Jr. 1983b, *ApJ*, 272, 54  
 ———. 1992a, *ApJ*, 388, 310  
 ———. 1992b, *ApJS*, 79, 255  
 ———. 1998, *ARA&A*, 36, 189  
 Landolt, A. U. 1992, *AJ*, 104, 340  
 Landy, S. D., & Szalay, A. S. 1993, *ApJ*, 412, 64  
 Leauthaud, A., et al. 2007, *ApJS*, 172, 219  
 Le Floc’h, E., et al. 2005, *ApJ*, 632, 169



- Lequeux, J. 1971, *A&A*, 15, 42
- Lilly, S. J., Le Fèvre, O., Hammer, F., & Crampton, D. 1996, *ApJ*, 460, L1
- Ly, C., et al. 2007, *ApJ*, 657, 738
- Madau, P., Ferguson, H. C., Dickinson, M. E., Giavalisco, M., Steidel, C. C., & Fruchter, A. 1996, *MNRAS*, 283, 1388
- Massarotti, M., Iovino, A., & Buzzoni, A. 2001, *ApJ*, 559, L105
- Meurer, G. R., et al. 2006, *ApJS*, 165, 307
- Miyazaki, S., et al. 2002, *PASJ*, 54, 833
- Mobasher, B., et al. 2007, *ApJS*, 172, 117
- Moorwood, A. F. M., van der Werf, P. P., Cuby, J. G., & Oliva, E. 2000, *A&A*, 362, 9
- Murayama, T., et al. 2007, *ApJS*, 172, 523
- Niklas, S., et al. 1997, *A&A* 322, 19
- Norberg, P., et al. 2001, *MNRAS*, 328, 64
- Ouchi, M., et al. 2004, *ApJ*, 611, 685
- . 2005, *ApJ*, 635, L117
- Pascual, S., Gallego, J., Aragón-Salamanca, A., & Zamorano, J. 2001, *A&A*, 379, 798
- Peebles, P. J. E. 1980, *The Large-Scale Structure of the Universe* (Princeton: Princeton Univ. Press)
- Pérez-González, P. G., Zamorano, J., Gallego, J., Aragón-Salamanca, A., & Gil de Paz, A. 2003, *ApJ*, 591, 827
- Sauvage, M., & Thuan, T. X. 1992, *ApJ*, 396, L69
- Schechter, P. 1976, *ApJ*, 203, 297
- Schminovich, D., et al. 2005, *ApJ*, 619, L47
- Scoville, N. Z., et al. 2007, *ApJS*, 172, 523
- Sopp, H. M., & Alexander, P. 1991, *MNRAS*, 251, 14
- Sullivan, M., Treyer, M., Ellis, R. S., Bridges, B., & Donas, J. 2000, *MNRAS*, 312, 442
- Takahashi, M., et al. 2007, *ApJS*, 172, 456
- Taniguchi, Y., et al. 2005, *PASJ*, 57, 165
- . 2007, *ApJS*, 172, 9
- Teplitz, H. I., Collins, N. R., Gardner, J. P., Hill, R. S., & Rhodes, J. 2003, *ApJ*, 589, 704
- Tresse, L., & Maddox, S. 1998, *ApJ*, 495, 691
- Tresse, L., Maddox, S., Le Fèvre, O., & Cuby, J.-G. 2002, *MNRAS*, 337, 369
- Tresse, L., Maddox, S., Loveday, J., & Singleton, C. 1999, *MNRAS*, 310, 262
- Tresse, L., Rola, C., Hammer, F., Stasińska, G., Le Fèvre, O., Lilly, S. J., & Crampton, D. 1996, *MNRAS*, 281, 847
- Treyer, M. A., Ellis, R. S., Milliard, B., Donas, J., & Bridges, T. J. 1998, *MNRAS*, 300, 303
- Wilson, G., Cowie, L. L., Barger, A., & Burke, D. J. 2002, *AJ*, 124, 1258
- Yan, L., et al. 1999, *ApJ*, 519, L47
- Zehavi, I., et al. 2004, *ApJ*, 608, 16
- . 2005, *ApJ*, 630, 1